

A Structural Battery and its Multifunctional Performance

Leif E. Asp,* Karl Bouton, David Carlstedt, Shanghong Duan, Ross Harnden, Wilhelm Johannisson, Marcus Johansen, Mats K. G. Johansson, Göran Lindbergh, Fang Liu, Kevin Peuvot, Lynn M. Schneider, Johanna Xu, and Dan Zenkert

Engineering materials that can store electrical energy in structural load paths can revolutionize lightweight design across transport modes. Stiff and strong batteries that use solid-state electrolytes and resilient electrodes and separators are generally lacking. Herein, a structural battery composite with unprecedented multifunctional performance is demonstrated, featuring an energy density of 24 Wh kg^{-1} and an elastic modulus of 25 GPa and tensile strength exceeding 300 MPa. The structural battery is made from multifunctional constituents, where reinforcing carbon fibers (CFs) act as electrode and current collector. A structural electrolyte is used for load transfer and ion transport and a glass fiber fabric separates the CF electrode from an aluminum foil-supported lithium-iron-phosphate positive electrode. Equipped with these materials, lighter electrical cars, aircraft, and consumer goods can be pursued.

1. Introduction

Lightweight electrical energy-storage systems are required to meet the ever-growing needs of electrification across transport modes and consumer goods.^[1,2] Current battery systems add weight with no contribution to the system's structural

performance. For instance, the battery of the Tesla model S (85 kWh) weighs $\approx 25\%$ of the total vehicle weight.^[3] For electric vehicles to be more efficient, and for all-electric aircraft to evolve, total energy storage must be increased while maintaining or reducing weight.^[4] This article addresses an alternative approach to realize efficient electrically powered systems. Here, the electrical energy storage is integrated in the structural material of the vehicle—via multifunctional materials coined as “structural battery composites or structural power composites.”^[5–8] Electrical energy storage in structural load paths has been shown to offer large mass savings for cars, aircraft, consumer electronics, etc.^[9–15] Due to their multifunc-

tionality, structural battery composites are often referred to as “mass-less energy storage” and have the potential to revolutionize the future design of electric vehicles and devices.


The first attempt to make a laminated structural battery composite was by the US Army Research Laboratory (ARL) in 2007.^[16] They used a carbon fiber (CF) lamina as a negative electrode and a metal mesh coated with a cathode material as positive electrode, separated by a glass fiber (GF) fabric. The structural battery composite showed promising mechanical performance but could not store electrochemical energy due to poor electrical insulation. Liu et al. suggested a structural battery composite using short CF-reinforced electrodes combined with a solid-state polymer electrolyte matrix.^[17] The CFs were electrochemically inactive and only used as reinforcement. However, they were not able to manufacture the short fiber electrodes as intended, nor were they able to identify a solid-state electrolyte with sufficiently high ionic conductivity. Instead they used a gel electrolyte, resulting in a battery with a low tensile modulus, of $\approx 3 \text{ GPa}$. The battery demonstrated an energy density of 35 Wh kg^{-1} . Inspired by these works, the authors of the current study engaged in the development of structural battery composites. In a first attempt, Ekstedt et al. made a functioning laminated structural battery using a gel electrolyte reinforced with a CF weave negative electrode, a glass weave separator, and a lithium-iron-phosphate (LFP)/aluminum fiber weave positive electrode.^[18] No experimental data on the electrochemical capacity or mechanical properties were reported. However, the mechanical properties are expected to have been poor, given the use of a very soft matrix material. In fact, electrolytes with a low Young's modulus (few MPa or less) cannot be used to realize structural batteries as they do not allow efficient mechanical load transfer between fibers.

Prof. L. E. Asp, D. Carlstedt, S. Duan, M. Johansen, Dr. F. Liu, Dr. J. Xu
Department of Industrial and Materials Science
Chalmers University of Technology
Gothenburg SE-412 96, Sweden
E-mail: leif.asp@chalmers.se

K. Bouton, R. Harnden, Dr. W. Johannisson, Prof. D. Zenkert
Department of Engineering Mechanics
KTH Royal Institute of Technology
Stockholm SE-100 44, Sweden

Prof. M. K. G. Johansson, L. M. Schneider
Department of Fibre and Polymer Technology
KTH Royal Institute of Technology
Stockholm SE-100 44, Sweden

Prof. G. Lindbergh, K. Peuvot
Department of Chemical Engineering
KTH Royal Institute of Technology
Stockholm SE-100 44, Sweden

 The ORCID identification number(s) for the author(s) of this article can be found under <https://doi.org/10.1002/aesr.202000093>.

© 2021 The Authors. Advanced Energy and Sustainability Research published by Wiley-VCH GmbH. This is an open access article under the terms of the Creative Commons Attribution License, which permits use, distribution and reproduction in any medium, provided the original work is properly cited.

DOI: 10.1002/aesr.202000093

Load transfer between reinforcing fibers is a key feature of the matrix material in any structural composite.

To move away from soft electrolytes, Carlson^[19] made a laminated structural battery component using a bicontinuous multifunctional polymer/ionic liquid electrolyte matrix, developed for structural supercapacitors by Shirshova et al.^[20] The structural battery was made from an IMS65 CF-woven fabric negative electrode and an LFP-coated metal foil positive electrode, separated by a glass fabric. The stack was impregnated with the multifunctional polymer/ionic liquid electrolyte system, which phase separated during cure. The structural battery was used to light an LED, but no multifunctional material data were reported.^[19] A similar approach was taken by Yu et al. to make structural battery negative half cells.^[21] The laminated structural battery half cells were made from T700 CF electrodes in a bicontinuous epoxy/ionic liquid structural electrolyte. The half cells were made into coin cells and electrochemically cycled versus lithium (Li) metal. A first discharge capacity in the range of 12–25 mAh g⁻¹ was reported and the samples experienced significant capacity losses after continued cycling. Stiffness data presented for the structural battery half cells were along the fiber direction and hence dominated by the CFs.

Recently, a bicontinuous polymer electrolyte system, referred to as a structural battery electrolyte (SBE), was developed for structural battery composites by Ihrner et al.^[22] and later optimized for manufacturing by Schneider et al.^[23] The SBE consists of a porous methacrylate polymer (for mechanical load transfer) impregnated with a liquid electrolyte mixture containing Li salt for ionic conductivity. The SBE has a Young's modulus around 0.5 GPa and an ionic conductivity of 2×10^{-4} S cm⁻¹. Johannisson et al. demonstrated highly promising electrochemical and mechanical performance using this SBE in CF electrode half cells.^[7] Moreover, the SBE matrix was found to sustain the volume change of CF as the mechanical properties were unaffected by electrochemical cycling. A similar SBE is used in the current study.

In a recent study, Moyer et al. reported on yet another type of CF-reinforced structural Li-ion battery composite.^[24] The battery did not exploit the electrochemical capability of CFs. Instead, the active material in the negative electrode was graphite and LFP was used as active material in the positive electrode. The CF composite-supported electrode laminae were separated by a Whatman GF separator soaked in a liquid electrolyte. Consequently, no mechanical loads can be transferred in the electrochemically active region of the CF-reinforced Li-ion battery composite. Moyer et al. reported an energy density surpassing 35 Wh kg⁻¹. They further demonstrate a low Young's modulus of around 2 GPa (they report 2 MPa but the data suggest that this is a misprint).^[24]

The work on structural battery composites to date either presents good electrochemical or mechanical performance. No study has yet demonstrated good combined properties. Furthermore, no structural battery with an elastic modulus greater than that of a glassy polymer has been reported. Also, mechanical data provided in previous work only present stiffness and strength data in the fiber direction (which is the stiff and strong direction) and not in the direction perpendicular to the fibers. Finally, most previous studies do not fully exploit multifunctional material constituents. For example, fiber

reinforcement adds stiffness and strength and acts as a current collector, but is not electrochemically active, or a liquid electrolyte that cannot transfer mechanical loads is used.

In this article, we propose a structural battery composite material made from multifunctional material constituents and demonstrate its multifunctional performance. The structural battery composite consists of a CF negative electrode and an aluminum film-supported positive electrode separated by a GF separator in a SBE matrix material. Consequently, the CFs act as host for Li (i.e., active electrode material), conduct electrons, and reinforce the material. Similarly, the positive electrode foil provides combined mechanical and electrical functionality. The SBE facilitates Li-ion transport and transfers mechanical loads between fibers, particles, and plies. Two types of GF fabric separators, a Whatman GF/A and a GF plain weave, are used as model materials to investigate the effects of separator thickness and architecture, as well as material anisotropy, on the multifunctional performance. The structural battery composite full cells are fabricated, as shown in Figure 1.

2. Results and Discussion

2.1. Structural Battery Microstructures

The structural battery composites were studied in a scanning electron microscope (SEM). Micrographs of the cells with the two different separators are shown in Figure 2. Due to the applied pressure during thermal curing, the thickness of both separators is significantly thinner than their original thickness. The average thickness of the Whatman GF/A separator is 185 μ m, whereas it is 70 μ m for the GF plain weave separator. Unlike the relatively constant separator thickness, the CF electrode thickness varies dramatically across the width of the structural battery cell. The fiber volume fraction varies within the negative electrode but is on average $\approx 20\%$. The variation in the CF electrode thickness is inherent to the manual manufacturing process.

Moreover, it is evident from Figure 2 that the appearance of the CF electrode differs between the two separator solutions. This will affect the local properties of the electrode lamina (e.g., conductivities) which will influence the electrochemical performance of the cell.

2.2. Electrochemical Performance

The specific capacities and energy densities of the tested structural battery cells are shown in Table 1.

The nominal voltage during discharge was ≈ 2.8 V for both cell types. The energy densities at 0.05 C (i.e., a discharge time of ≈ 20 h) of the battery cells utilizing the Whatman GF/A and GF plain weave separator are 11.6 and 23.6 Wh kg⁻¹, respectively. These numbers are based on the total mass of the battery cell (i.e., accounting for the mass of the electrodes, separator, SBE, and current collectors in the cell). The corresponding energy densities, when only accounting for mass of the active electrode materials (i.e., CFs and LFP particles), are 90.1 and 106 Wh kg⁻¹, respectively. In Table 1 the calculated maximum energy densities for the two cells are reported. The maximum energy density with respect to the active material is the same

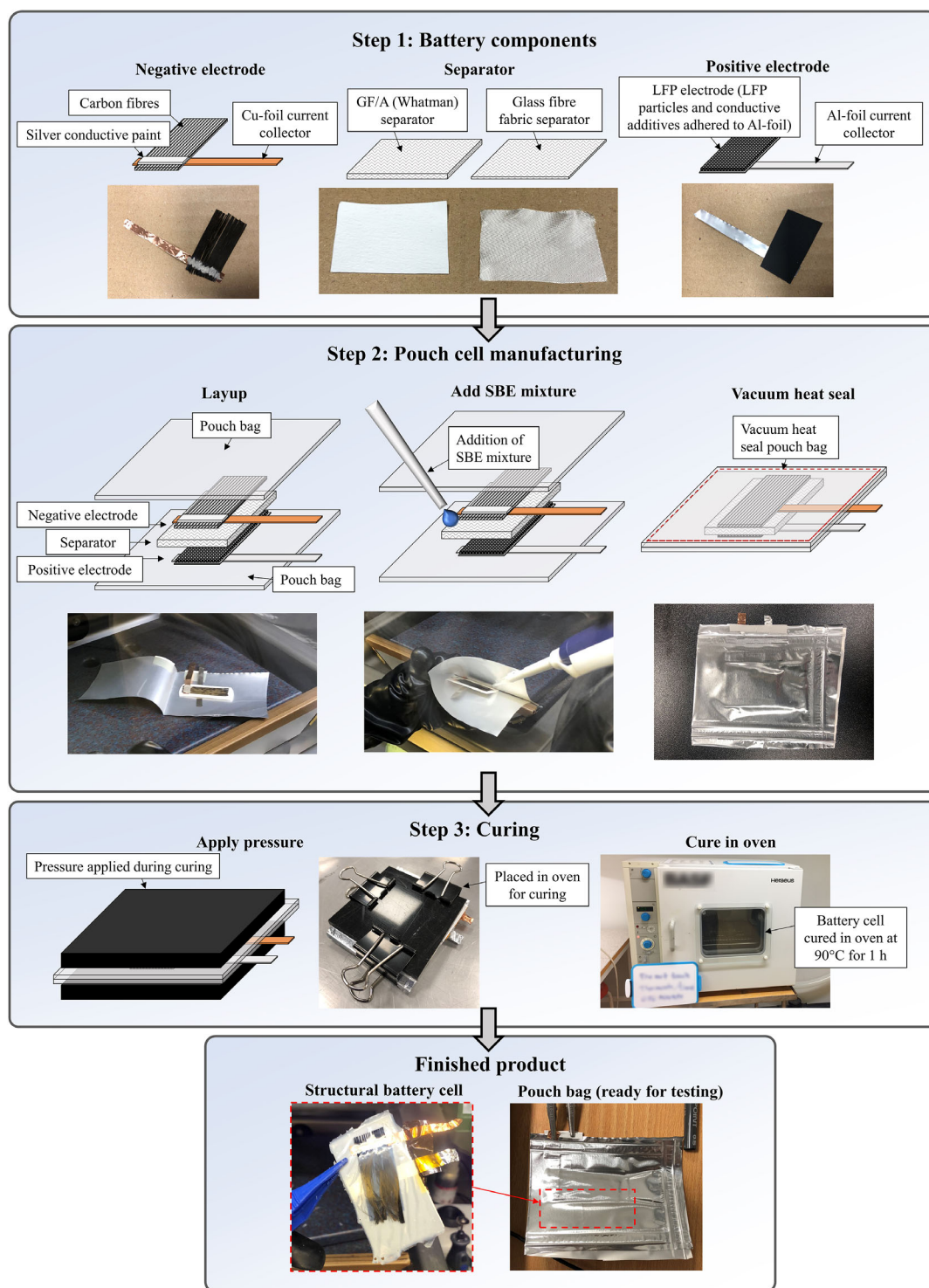


Figure 1. Structural battery composite fabrication, showing the steps: battery component manufacture, pouch-cell manufacture, and curing of the SBE.

for the two cell types. The difference in measured energy density with respect to active material mass for the two structural battery cells is related to the dissimilar separator thickness and is explained by the higher internal resistance of the structural battery with the thicker Whatman GF/A separator, resulting in a

lower utilization of the electrodes' maximum available capacities. Furthermore, the specific powers for the two cells at 3 C are 5.94 and 9.56 W kg⁻¹, respectively. With respect to the active electrode materials, the specific power is 34.7 W kg⁻¹. All tested battery cells showed similar electrochemical performances.

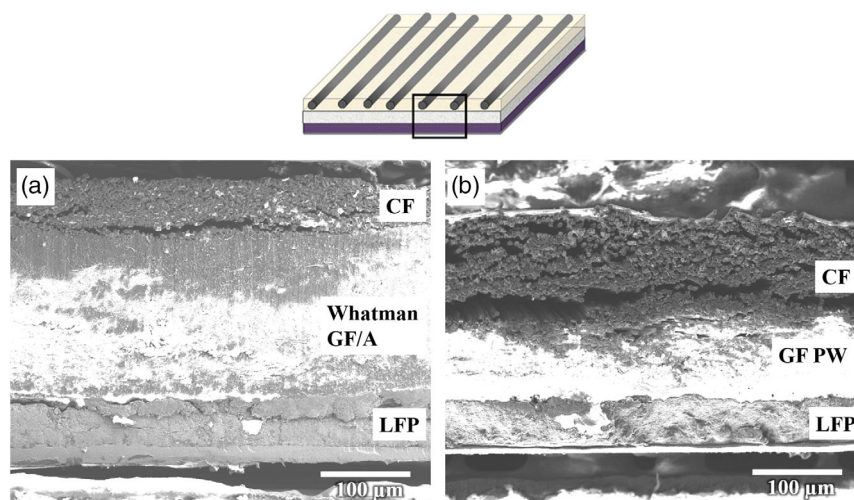


Figure 2. SEM micrographs of the structural batteries' cross sections, as indicated by the inscribed box in the schematic. Structural battery cross sections with a) Whatman GF/A separator and b) GF plain weave separator. Average thicknesses in the regions depicted in the micrographs: a) CF electrode, 65 μm ; Whatman GF/A separator, 185 μm ; and positive (LFP) electrode, 50 μm ; b) CF electrode, 125 μm ; GF separator, 70 μm ; and positive (LFP) electrode, 50 μm .

Table 1. Representative specific capacities and energy densities of the tested structural battery cells at 0.05 C (i.e., a discharge time of ≈ 20 h), as well as the calculated maximum energy densities, with a nominal voltage during discharge of 2.8 V. Specific power at 3 C with a nominal voltage during discharge of 2.48 V. "Battery cell" corresponds to the case where the total mass of battery cell is accounted for (i.e., accounting for all constituents) whereas "Active mat." represents values where only the mass of the active electrode materials is accounted for (i.e., CFs and LFP particles).

Separator	Whatman GF/A		GF plain weave	
	Battery cell	Active mat.	Battery cell	Active mat.
Specific capacity [Ah kg^{-1}]	4.13	32.2	8.55	38.4
Energy density [Wh kg^{-1}]	11.6	90.1	23.6	106
Calculated maximum energy density [Wh kg^{-1}]	37.7	220	60.6	220
Specific power [W kg^{-1}]	5.94	34.7	9.56	34.7
Total mass of cell [g cm^{-2}]	0.074		0.046	
Cell thickness [mm]	0.40		0.27	

The electrochemical performance of a structural battery composite with a Whatman GF/A separator is shown in Figure 3. Figure 3a shows the typical charge/discharge voltage profiles of the structural battery cells during galvanostatic cycling at different C rates. The voltage profiles indicate a stable charge/discharge process at the different C rates and a relatively balanced cell. Moreover, in Figure 3b, the energy density for a structural battery cell with the Whatman GF/A separator is presented for different C rates. It is evident that the capacity fade is negligible within the given cycling process and stable energy densities at different C rates are demonstrated. Furthermore, good capacity retention is observed over long-term cycling at 1 C (Figure 3c). It should be noted that the battery cell has been cycled for 35 cycles (i.e., preconditioning and cycle scheme shown in Figure 3b) prior

to the cycling procedure, as shown in Figure 3c. Hence, the cell shows high capacity retention even after more than 60 charge/discharge cycles. Finally, Figure 3d shows the energy density versus the C rate for both separator alternatives. Notably, the energy density of the structural battery with the GF plain weave separator is significantly higher than that of the cell with the thicker Whatman GF/A separator. In general, the electrochemical performance is limited by the mass of the active materials relative to the total mass. For these structural batteries, the performance is limited by the excessive amount of SBE. This can be mitigated by an improved manufacturing process that allows for more evenly distributed CFs and higher fiber volume fraction, i.e., increased volume fraction of active material, in the negative electrode.

2.3. Mechanical Performance

The mechanical properties of the structural batteries were characterized under tensile loading in both x - and y -directions, as shown in Figure 4. The GF plain weave separator was placed with the fibers extending either in $\pm 45^\circ$ or $0^\circ/90^\circ$ directions, where the 0° direction is parallel to the x -direction. The average elastic moduli and the tensile strengths of the laminated full cells are shown in Table 2.

Representative load–displacement curves for all three specimen types and loading directions are shown in Figure 4. The modulus is highest in the x -direction for all structural battery composites, see E_x in Table 2. Furthermore, a linear force–displacement relationship in the x -direction is found for all samples, see Figure 4d. The high modulus and linear response are expected as the stiff CFs in the negative electrode are oriented parallel to the loading direction. The highest modulus, E_x , is found for the $0^\circ/90^\circ$ GF plain weave separator structural battery composite. Again, this is explained by the beneficial orientation of the reinforcing fibers in the separator, i.e., the GFs extending

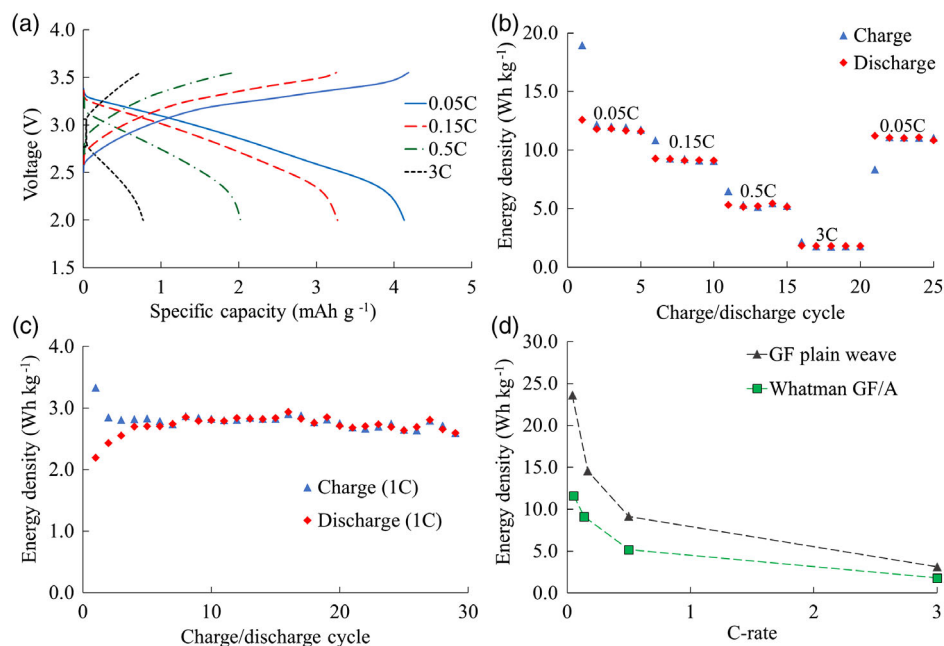


Figure 3. Results from electrochemical characterization based on the total weight of the battery cell. a) Voltage profile at different C rates. b) Energy density at different C rates. c) Long-term cycling (at 1 C). d) Energy density versus C rate for the two separator solutions. Note that the C rates are defined with respect to the capacity of the tested battery cells.

in the 0° direction. Hence, the CFs in the negative electrode and the GFs extending in the 0° direction both reinforce the battery composite to their maximum in this particular composite and for this load direction.

In contrast, the modulus in the y -direction, E_y , is generally lower. This is explained by the matrix-dominated response of the composite to tensile loads in the y -direction. The moduli in the y -direction for the structural batteries made from the $\pm 45^\circ$ -oriented GF plain weave and the Whatman GF/A separators are quite low compared with 0°/90°, which is a much more favorable configuration. In Figure 4e, a conspicuous nonlinear force–displacement response is observed. This is particularly pronounced for the $\pm 45^\circ$ -oriented GF plain weave separator structural battery as this composite sustains substantial shear loads (i.e., scissoring of the weave).

As discussed in the Experimental Section, the tensile strength results may be impaired by premature failure inherent to surface defects or stress concentrations in the clamping region. In fact, most of the specimens failed at the grips. Consequently, the strength values reported in Table 2 should be considered as lower bounds of strength for the tested structural battery composites. The strengths of the specimen with the Whatman GF/A separator are typically half of those for the specimens with GF plain weave separator, both in the x - and y -directions. The highest recorded strength exceeds 312 MPa and is for the structural battery composite with the $\pm 45^\circ$ -oriented GF plain weave separator.

2.4. Multifunctional Performance

The structural battery composite demonstrates excellent multifunctional performance. The thinner GF plain weave separator

results in a lighter structural battery cell, as the amount of separator material and SBE is greatly reduced. As a consequence, the energy density is more than doubled—it increases from 11.6 to 23.6 Wh kg⁻¹. Moreover, the improvement in electrochemical performance comes in hand with enhanced mechanical performance as the elastic modulus is increased by almost 40% (from 18.3 to 25.4 GPa) and 360% (from 2.9 to 13.3 GPa) in the x - and y -directions, respectively. Thus, both the electrochemical and mechanical performance can be dramatically improved replacing the Whatman GF/A separator with the significantly thinner and stiffer GF plain weave fabric.

Further improvements can likely be achieved. First, using thinner separators will reduce the mass of the structural battery as the amount of SBE is also reduced. This will immediately result in increased energy density and elastic modulus. The increased elastic modulus results from the increase in the relative thickness of the stiffer CF lamina. The current structural battery composite designs are generally less stiff than expected for a CF-reinforced composite. In particular, elastic modulus in the x -direction appears to be on the low side. There are at least three reasons for this. First, the fiber volume fraction in the negative electrode is lower than desired and limited by the manufacturing method and can probably be improved significantly using, e.g., a vacuum-infusion manufacturing method.^[25] Second, due to the manual process, the CFs in the negative electrode are not ideally straight, which again may be remedied using fixtures to hold the spread tow fiber bundles during manufacturing. Finally, the stiff carbon fiber electrode constitutes only a part of the total laminate thickness, which is shown in the micrograph of the structural battery composite with the Whatman GF/A separator shown in Figure 2a. Thinner separators is the key approach to improve this.

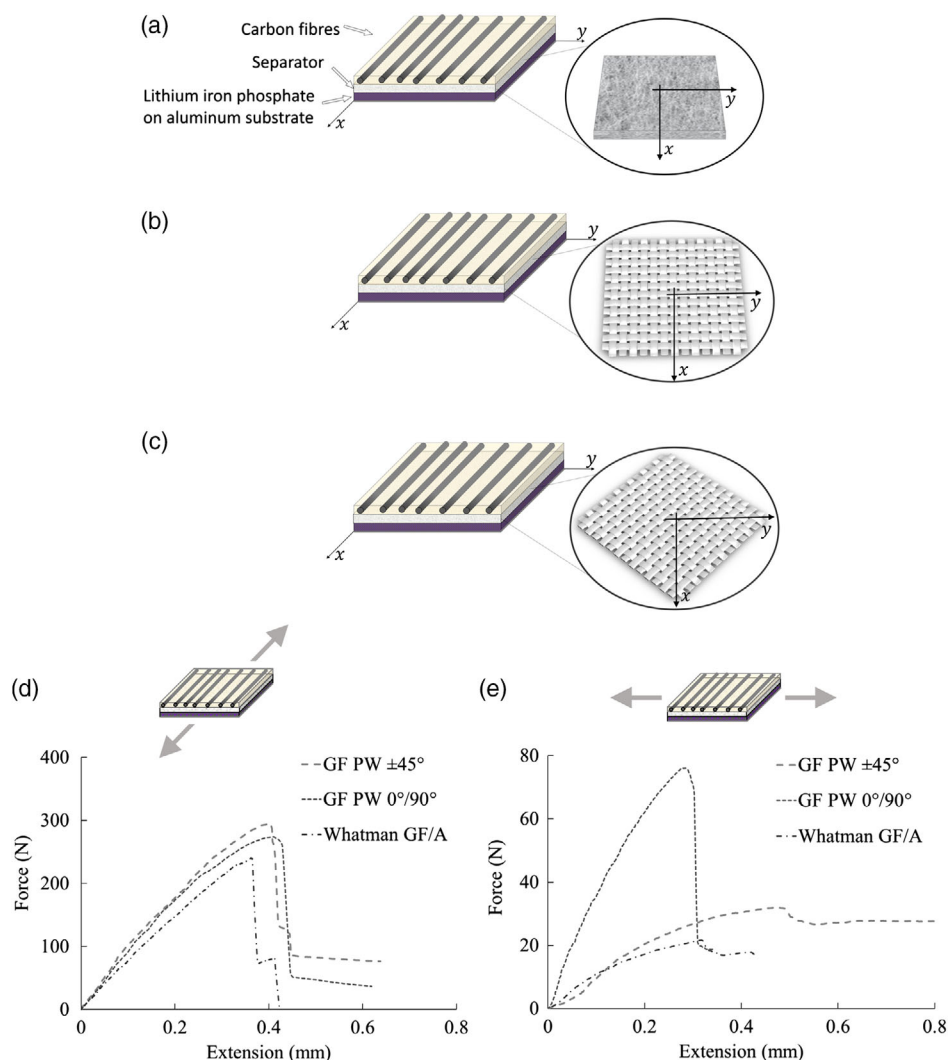


Figure 4. The structural battery full cell laminates and their mechanical response. Schematics showing the orientation of the separator fabrics relative to the loading directions: a) Whatman GF/A; b) GF plain weave with its warp and weft yarns oriented in $0^\circ/90^\circ$; and c) GF plain weave with its warp and weft yarns oriented in $\pm 45^\circ$. Representative load–displacement curves from tensile tests. d) Loading in the x-direction and e) loading in y-direction.

Table 2. Mechanical properties from tensile tests of the structural battery laminates. E_x and E_y are the elastic moduli in the x- and y-directions, respectively. X and Y are the tensile strengths in the x- and y-directions, respectively. Note that the reported strength values are considered lower bounds due to limitations in the sample preparation process, as discussed in Experimental Section.

Property	Separator type		
	Whatman GF/A	GF plain weave $\pm 45^\circ$	GF plain weave $0^\circ/90^\circ$
E_x [GPa]	18.3(± 0.9)	14.6(± 0.6)	25.4(± 3.3)
E_y [GPa]	2.9(± 0.5)	2.8(± 0.2)	13.3(± 0.7)
X [MPa]	>163	>312	>287
Y [MPa]	>16	>34	>72

The elastic modulus of the structural batteries presented here ranges over an order of magnitude at maintained electrochemical

performance. Within this selection of materials, the GF plain weave separators oriented in $\pm 45^\circ$ and $0^\circ/90^\circ$ demonstrate lower and upper bounds for the possible variation in modulus without affecting the electrochemical performance. Consequently, requirements on mechanical performance for given applications can be met by clever selection of fiber orientations and lay-up.

Until now only a few studies reporting the multifunctional performance of structural batteries have been published. Hopkins et al. presented an overview of the work to date.^[26] Among the studies cited only a handful consider structural battery composites, which they refer to as coupled structural batteries. Furthermore, almost all of these demonstrate poor multifunctional performance, where either the electrical or the mechanical performance is prioritized. For example, Thakur and Dong^[27] reported an energy density of 24 Wh kg^{-1} at an elastic modulus of only 0.29 GPa, whereas Meng et al.^[28] demonstrated a structural battery material with an elastic modulus of

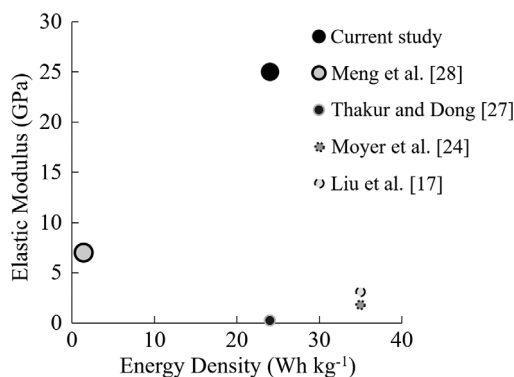


Figure 5. Elastic modulus and cell level energy density of reported structural battery composites, numbered by their references.

7.0 GPa but a low energy-storage capability of 1.4 Wh kg⁻¹. Moyer et al. reported a multifunctional device, exploiting CFs as collectors.^[24] Use of a liquid electrolyte generated a high energy density (35 Wh kg⁻¹) but resulted in an inferior elastic modulus (2 GPa). Liu et al. reported an energy density of 35 Wh kg⁻¹ and an elastic modulus of 3 GPa.^[17] The relatively high energy density can be partly explained by the fact that they used LiCoO₂, which has a higher specific capacity than LFP, as the active material in the positive electrode. It is also not clear, however, if the energy density reported is relative to the mass of the entire cell or the active materials, nor is the charging history for the cell given.

The multifunctional properties of structural battery composites made to date are shown in **Figure 5**. It is evident that no previous structural battery has been made that matches the multifunctional performance of the structural battery composite presented in the current study.

The structural battery composite is contained in a pouch bag as described in the Experimental Section. To further illustrate the electrochemical and mechanical functions, the structural battery composite is extracted from the pouch bag inside the glovebox and connected to an LED. A video demonstrating the electrochemical function under handling and gentle mechanical bending is presented in Supporting Information. Two still shots from the video are shown in **Figure 6**.

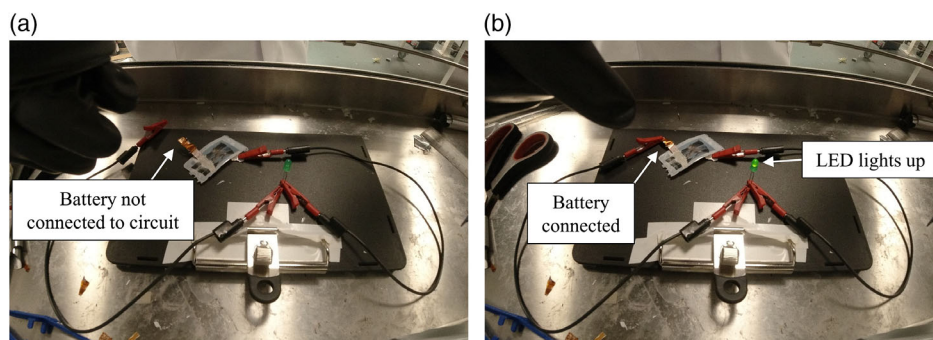


Figure 6. Images from video (available as Supporting Information) showing the structural battery cell without the pouch bag lighting an LED inside the glovebox while exposed to mechanical loading. a) Before the cell is connected to the circuit (LED light off) and b) when connected to circuit (LED light on).

3. Conclusion

Structural battery composite materials, exploiting multifunctional constituents, have been realized and demonstrate an energy density of 24 Wh kg⁻¹ and an elastic modulus of 25 GPa. Their combined electrochemical and mechanical properties outperform all previous structural battery materials reported in the literature. From the relationships found between the constituents and multifunctional performance of the structural battery composite, we have confirmed the importance of having thin and stiff separators and to increase the relative thickness of, as well as the fiber volume fraction in, the negative CF electrode. Armed with this understanding of the complementary, and sometimes counteracting, electrochemical and mechanical functions, future structural battery composites can be designed—where electrochemical energy density and elastic stiffness and mechanical strength can be tuned as desired.

4. Experimental Section

Materials: Ultrathin spread tow UD tapes of T800SC-12k-50C PAN-based CF with a linear tow weight of 0.52 g m⁻¹ were supplied by Oxeon AB, Sweden. The spread tow CF tapes had a width of 15 mm and were used as negative electrodes. The multifunctional properties of the T800 fiber are reported by, e.g., Kjell et al.^[29] and Fredi et al.^[30] Moreover, a battery-grade single-side LFP (LiFePO₄)-coated aluminum foil (82 μm thick; rated capacity of 1 mAh cm⁻²) positive electrode was purchased from Custom Cells Itzehoe GmbH, Germany. Two types of GF separators were used: 1) Whatman glass microfiber separator (Whatman GF/A, 260 μm thick) supplied by Sigma Aldrich and 2) a 0°/90° woven GF fabric (GF plain weave, style 1086), with a surface weight of 53 g m⁻² (≈50 μm thick), manufactured by Gividi Fabrics s.r.l., Italy, and supplied by Isola Group, Europe. The bicontinuous SBE included the following constituents: for the polymer material part Bisphenol A ethoxylate dimethacrylate (M_n: 540 g mol⁻¹) was supplied by Sartomer Europe; for the liquid electrolyte part, propylene carbonate (PC) (99% anhydrous, acid <10 ppm, H₂O <10 ppm) and ethylene carbonate (EC) (99% anhydrous) supplied by Sigma Aldrich were used. Furthermore, for the SBE lithium trifluoromethanesulfonate (LiTf) (99.99%), lithium bis(oxalato)borate (LiBoB) and 2,2'-azobis(2-methylpropionitrile) (AIBN) purchased from Sigma Aldrich were used. All materials were used as received.

Structural Battery Full Cell Preparation: An illustrative overview of the structural battery composite full cells manufacture is shown in Figure 1. The negative electrode was made from a CF spread tow and the positive electrode was a commercially available LFP electrode foil. Both electrodes were cut in dimensions of 30 × 15 mm². This corresponded to ≈19 mg of CFs and 38 mg of LFP particles in the complete

battery cell. A copper foil current collector was adhered to the CFs using silver conductive paint. An aluminum current collector was placed on the aluminum side of the LFP foil. Two types of separators were used: 1) one made from Whatman GF/A and 2) one made from a stack of two 0°/90° woven GF fabrics (denoted GF plain weave). Both separators were cut slightly larger than the electrodes ($\approx 50 \times 20 \text{ mm}^2$) to ensure that the electrodes did not come in direct contact (to avoid short circuit). The battery cell stack was then placed inside a pouch laminate bag (PET/Al/PE, 12 μm /9 μm /75 μm thick) to protect the electrochemical cell from air and moisture. The battery cell stack was then impregnated with an SBE mixture using a pipet before the pouch bag was vacuum heat sealed. The SBE mixture was prepared in accordance with the procedure described in the study by Schneider et al.,^[23] with the only differences being that DMMP in the electrolyte was replaced with PC, the mixing ratio of monomer versus liquid electrolyte was taken, and that a LiBoB salt was added to prevent unwanted side reactions induced by the exclusive use of LiTf, as discussed in Supporting information. The SBE solution was made by mixing 50:50 wt % of 1) a liquid electrolyte solution made from the mixture of LiBoB and LiTf at concentrations of 0.4 and 0.6 M, respectively, in EC:PC 1:1 w/w (50:50 wt%) and 2) monomer bisphenol A ethoxylate dimethacrylate and the thermal initiator AIBN (1 wt% of the monomer weight). To achieve a homogeneous solution, the SBE mixture was stirred using a vortex before it was added to the battery cell. Once the pouch bag was vacuum heat sealed, it was transferred to a preheated oven outside the glovebox and thermally cured at 90 °C for 60 min. During thermal curing pressure was applied on the cells using clamps.

In total, 16 structural battery composite cells were manufactured and characterized for their multifunctional performance. Among these, 12 were made using a Whatman GF/A separator and 4 with the GF plain weave separator.

Electrochemical Testing: The specific capacity of the structural battery full cells was measured by means of repeated galvanostatic charge and discharge cycles using a Neware CT-4008-5V10mA-164 battery cycler. The cells were cycled between 2.00 and 3.55 V using a series of current densities or C rates. Prior to the electrochemical characterization, the battery cells were cycled for ten complete charge/discharge cycles to precondition the cells. During this stage, the applied current density was set to 1.76 mA g^{-1} with respect to the mass of the active electrode materials (i.e., CFs and LFP particles) available in the battery cell. The electrochemical characterization was conducted after the preconditioning stage and the cells were cycled at current densities applied as follows: five complete charge/discharge cycles for each current step using 1.76, 3.51, 7.02, and 14.0 mA g^{-1} relative to the active electrode materials in the battery cell. This was found to be approximately equivalent to 0.05, 0.15, 0.5, and 3 C, with respect to the capacity of the tested battery cells. Between each charge and discharge cycle, a resting time of 60 min was used to allow ion-concentration gradients to relax. In total, eight battery cells were characterized electrochemically using the Whatman GF/A separator and two with the GF plain weave separator.

Mechanical Testing: Tensile tests were conducted to characterize the elastic properties of the laminate in x- and y-directions, as shown in Figure 4. Due to the dimensions of the full cell, measuring mechanical properties of the laminate presents certain limitations. For these specimens, the challenge lies in the strain measurement without the possibility of using conventional techniques such as digital image correlation or strain gauges. The microtester used for mechanical characterization, a Deben 2 kN tensile stage, further prevented use of conventional test standards, such as ASTM D3039. Instead, test specimens were adapted to fit the test equipment, with the dimensions $30 \times 3.3 \text{ mm}^2$ (length \times width).

Slender test specimens were cut from the manufactured structural battery cells with great caution to allow for precise measurement of the elastic modulus. Accurate measurement of composite strength, however, requires comprehensive sample preparation, involving polishing free edges and tabbing clamping regions to prevent premature failure and hence underestimated material strength. Such sample preparations were not possible here. Tensile tests were made on a minimum of five samples per specimen type. Mechanical tests were conducted on pristine structural battery cells, only, i.e., no electrochemical cycling was performed on the

samples prior to the mechanical test. Tensile tests were conducted under displacement control at a rate of 0.1 mm min^{-1} . Applied strain was calculated from the crosshead displacement of the microtester compensating for the machine compliance according to ASTM D3379 and is further described in Supporting Information.

Supporting Information

Supporting Information is available from the Wiley Online Library or from the author.

Acknowledgements

The authors would like to thank the following sources for funding this research: Swedish Energy Agency grant #37712-1; the Swedish Research Council, projects 2017-03898 and 621-2014-4577; the strategic innovation program SIP LIGHTer (funding provided by VNNova, the Swedish Energy Agency and Formas); H2020 Clean Sky II project SORCERER no. 738085 and work supported by the Air Force Office of Scientific Research under award numbers FA9550-17-1-0338 and FA9550-17-1-0244.

Conflict of Interest

The authors declare no conflict of interest.

Keywords

biomimetics, carbon fiber composites, fibrous materials, lithium-ion batteries, multifunctional materials, self-sustaining materials, solid states

Received: December 10, 2020

Revised: December 15, 2020

Published online: January 27, 2021

- [1] EARPA Position Paper, Materials, Design and Production Systems, Importance for European Road Transport Research and FP7, **2006**.
- [2] Flightpath 2050, Europe's Vision for Aviation, The European Commission, 2011, <https://doi.org/10.2777/50266> (accessed: November 2020).
- [3] Tesla Model S Owner's Manual, Version 2018.48.12, https://www.tesla.com/sites/default/files/model_s_owners_manual_north_america_en_us.pdf, (accessed: November 2020).
- [4] C. De Cauwer, J. van Mierlo, T. Coosemans, *Energies* **2015**, *8*, 8573.
- [5] L. E. Asp, E. S. Greenhalgh, *Compos. Sci. Technol.* **2014**, *101*, 41.
- [6] L. E. Asp, M. Johansson, G. Lindbergh, J. Xu, D. Zenkert, *Funct. Compos. Struct.* **2019**, *1*, 042001.
- [7] W. Johansson, N. Ihrner, D. Zenkert, M. Johansson, D. Carlstedt, L. E. Asp, F. Sieland, *Compos. Sci. Technol.* **2018**, *168*, 81.
- [8] F. Mo, G. Liang, Z. Huang, H. Li, D. Wang, C. Zhi, *Adv. Mater.* **2020**, *32*, 1902151.
- [9] J. P. Thomas, M. A. Qidwai, *JOM* **2005**, *57*, 18.
- [10] D. Carlstedt, L. E. Asp, *Composites, Part B* **2020**, *186*, 107822.
- [11] W. Johansson, D. Zenkert, G. Lindbergh, *Multifunct. Mater.* **2019**, *2*, 035002.
- [12] W. Johansson, S. Nguyen, G. Lindbergh, D. Zenkert, E. S. Greenhalgh, M. S. P. Shaffer, A. R. J. Kucernack, *Multifunct. Mater.* **2020**, *3*, 025002.

- [13] A. E. Scholz, A. Hermanutz, M. Hornung, in *Proc. Conf. 67. Dtsch. Luft- und Raumfahrtkongress*, DGLR, Friedrichshafen, Germany **2018**, pp. 1–12.
- [14] J. L. Lutkenhaus, P. Flouda, *Sci. Robot.* **2020**, 5, eabd7026.
- [15] Y. Chen, A. Amiri, J. G. Boyd, M. Naraghi, *Adv. Funct. Mater.* **2019**, 29, 1901425.
- [16] E. L. Wong, D. M. Baechele, K. Xu, R. H. Carter, J. F. Snyder, E. D. Wetzel, in *Proc. SAMPE 2007*, SAMPE, Baltimore, MD **2007**.
- [17] P. Liu, E. Sherman, A. Jacobsen, *J. Power Sources* **2009**, 189, 646.
- [18] S. Ekstedt, M. Wysocki, L. E. Asp, *Plast. Rubber Compos.* **2010**, 39, 148.
- [19] T. Carlson, *Doctoral Thesis*, **2013**.
- [20] N. Shirshova, H. Qian, M. S. P. Shaffer, E. S. Greenhalgh, P. T. Curtis, A. Kucernak, A. Bismarck, *Compos. Part A Appl. Sci. Manuf.* **2013**, 46, 96.
- [21] Y. Yu, B. Zhang, M. Feng, G. Qi, F. Tian, Q. Feng, J. Yang, S. Wang, *Compos. Sci. Technol.* **2017**, 147, 62.
- [22] N. Ihrner, W. Johannisson, F. Sieland, D. Zenkert, M. Johansson, *J. Mater. Chem. A* **2017**, 5, 25652.
- [23] L. Schneider, N. Ihrner, D. Zenkert, M. Johansson, *ACS Appl. Energy Mater.* **2019**, 2, 4362.
- [24] K. Moyer, C. Meng, B. Marshall, O. Assal, J. Eaves, D. Perez, R. Karkkainen, L. Roberson, C. L. Pint, *Energy Stor. Mater.* **2020**, 24, 676.
- [25] W. Johannisson, R. Harnden, D. Zenkert, G. Lindbergh, *PNAS* **2020**, 1921132117.
- [26] B. J. Hopkins, K. W. Long, D. R. Rolison, J. F. Parker, *Joule* **2020**, 4, 1.
- [27] A. Thakur, X. Dong, *Manuf. Lett.* **2020**, 24, 1.
- [28] C. Meng, N. Muralidharan, E. Teblum, K. E. Moyer, G. D. Nessim, C. L. Pint, *Nano Lett.* **2018**, 18, 7761.
- [29] M. H. Kjell, E. Jacques, D. Zenkert, M. Behm, G. Lindbergh, *J. Electrochem. Soc.* **2011**, 158, A1455.
- [30] G. Fredi, S. Jeschke, A. Boulaoued, J. Wallenstein, M. Rashidi, F. Liu, R. Harnden, D. Zenkert, J. Hagberg, G. Lindbergh, P. Johansson, L. Stievano, L. E. Asp, *Multifunct. Mater.* **2018**, 1, 015003.